Korean J. Chem. Eng., 35(3), 770-776 (2018)
DOI: 10.1007/s11814-017-0338-0

pISSN: 0256-1115
eISSN: 1975-7220

The effect of surfactants on the photocatalytic performance of BiOCl-ZnO nanoparticles in the degradation of an organic pollutant

Roshanak Halvaeifard and Shahram Sharifnia†

Catal. Res. Cen., Chem. Eng. Department, Razi University, Kermanshah 67149-67246, Iran
(*Received 13 October 2017 • accepted 3 December 2017*)

Abstract−The effect of surfactants on the performance of BiOCl-ZnO nanoparticles was investigated in the photocatalytic degradation of an organic pollutant. BiOCl-ZnO nanoparticles, modified with cetyl trimethyl ammonium bromide (CTAB) and polyethyleneglycol-20000 (PEG) as two kinds of surfactants, were used as photocatalysts. The photocatalysts were characterized by SEM, XRD, FTIR and DRS analyses. Characterization of the photocatalysts indicated the positive role of the surfactants in increasing the surface area of the photocatalysts. The experimental results demonstrated that PEG had more impressive effect than CTAB on the photocatalytic performance. The effects of important operational parameters, such as initial pollutant concentration, catalyst dosage and pH, on the degradation efficiency were studied. About 96.3% of the organic pollutant removal from synthetic wastewater was obtained at optimal conditions under visible irradiation. Equilibrium data were well fitted to the Langmuir isotherm equation.

Keywords: Photocatalytic Degradation, Organic Pollutant, Surfactant, BiOCl-ZnO Nanoparticles

INTRODUCTION

Many industries, such as plastics, textile, paper and pulp, generate waste water streams that contain a considerable amount of organic dyes. If these compounds are released into main water resources without any prior treatment, they can disturb the ecological balance in the environment. They have mutagenic and carcinogenic effects on aquatic organisms. Thus, at the end of the food chain, they are considered as a threat to human life. These contaminants are stable and non-biodegradable because of their chemical structure complications. Although there are several methods for water treatment, such as sedimentation, ion exchange, coagulation, adsorption, their use is limited due to their high operating costs [1,2].

Most recently, some alternative methods, including advanced oxidation processes (AOPs), have been widely applied for the purposes of treating. Their extensive applications are owing to their ability to remove non-biodegradable organic components, generate very reactive and oxidizing free radicals, especially hydroxyl radicals, and no need to dispose of residual sludge [3-8]. Among these alternative methods, the photocatalytic process proves its potential in mineralizing toxic organic and inorganic compounds in either liquid or gas phases [9]. The popularity of this process in environmental remediation is due to its non-toxic nature, low operating cost and high efficiency. Semiconductor photocatalysts play a key role in this regard [10].

In recent years, BiOX (X=Cl, Br, I), as new types of semiconductor materials, have attracted attention for environmental treatment due to their uniquely layered structure, chemical stability and outstanding photocatalytic activity [11-17]. They exhibit several excellent chemical and physical properties, such as optical, electrical, anisotropic structural, luminescent and mechanical properties, and have been extensively used in cosmetics, solar cells and photoelectrochemical devices [18]. A substantial number of experiments have indicated that BiOX semiconductors display stronger photocatalytic performance than TiO_2 (P25, Degussa) in degrading organic pollutants under UV-vis light irradiation [19]. Zhang et al. [20] revealed that BiOCl exhibited better performance than TiO_2 (P25) in the photocatalytic degradation of methyl orange (MO) dye at three-cycles. Simultaneously, they discussed the electronic band structure of BiOCl while using first-principles methods based on the density functional theory (DFT) [20]. They found that the open crystal structure and the indirect optical transition of BiOCl played crucial roles in its excellent photocatalytic activity [18,20-22].

The inability of absorbing visible light is one of the most important defects of these compounds. Coupled with metal oxide semiconductors, along with surfactants having polymeric matrix, is a potential strategy to deal with this problem. Dominant advantages of these nanocomposites include excellent corrosion strength, low density, good fatigue resistance, low thermal expansion and desirable thermal insulation.

As a result, we selected BiOCl from other bismuth oxyhalides, as an effectual photocatalyst, for degrading organic dyes due to its high activity and low recombination rate of photogenerated electrons and holes [23]. Moreover, for improving photonic applications of BiOCl in ultraviolet-visible (UV-vis) region, and constructing a visible-driven photocatalyst, it was coupled with ZnO/surfactant composites [24,25]. The influence of polyethylene glycol-20000 (PEG) and Cetyltrimethyl ammonium Bromide (CTAB), as two types of surfactants, was investigated on BiOCl-ZnO nanoparticle performance for the first time. Also, the influences of parameters, such as pH, initial pollutant concentration and dosage of photocatalyst, were evaluated on the degradation of the organic pollutant.

†To whom correspondence should be addressed.
E-mail: sharif@razi.ac.ir

MATERIALS AND METHODS

1. Materials

The reactants used in this study, such as bismuth nitrate pentahydrate ($Bi(NO_3)_3 \cdot 5H_2O$), potassium chloride (KCl), zinc nitrate hexahydrate ($Zn(NO_3)_3 \cdot 6H_2O$), sodium chloride (NaCl), Polyethylene glycohol-20000 (PEG), Cetyltrimethyl ammonium Bromide (CTAB), Methylene blue (MB) as an adsorbate (Methylene blue (C16H18N3SCl), a basic blue dyestuff with CI Classification No. 52015), accompanied by distilled water as solvent, were all purchased from Merck Co.

2. Photocatalyst Preparation

ZnO powder was synthesized via the precipitation method. First, 2.0 g of zinc nitrate and 1.0 g of the surfactant were dissolved in water. Next, sodium hydroxide solution (0.5 M) was slowly added into the above solution during 15 min. After that, the resultant suspension was heated to 50 °C for 1.5 h. Vigorous stirring was applied during the addition of NaOH. The precipitate was separated by centrifuge, washed with distilled water, and finally dried at 70 °C for 24 h in a vacuum dryer.

BiOCl nanoparticles were prepared according to the method proposed by Jiang et al. [26]. In detail, 1.0 mmol of $Bi(NO_3)_3 \cdot 5H_2O$ and 1.0 mmol of KCl were added in 15 mL of distilled water at room temperature.-After that, the slurry was stirred for 30 min, and then poured into a Teflon-lined stainless autoclave. The autoclave was heated at 160 °C for 24 h under autogenous pressure, and then cooled to room temperature. The resulting sediments were collected, thoroughly washed with ethanol and deionized water, and dried at 60 °C in air.

For preparation of BiOCl-ZnO-Surfactant photocatalyst, 1.0 g of BiOCl white powder and 1.0 g of ZnO powder were dissolved in water. The suspension was maintained under vigorous stirring for 24 h. Eventually, the composed sediment was separated by a centrifuge, and dried at 70 °C for 10 h.

3. Photocatalyst Characterization

The morphology and particle size of the samples were analyzed by field emission scanning electron microscopy (FESEM, Leo 440i). The crystallography and phase structure of the composites were identified by X-ray diffraction (XRD, PANalytical X'Pert Pro, Cu-Kα: λ=0.154 nm). Fourier transform infrared (FT-IR) spectra were recorded using Alpha FTIR spectrometer (Burker in Germany) at room temperature. Also, UV-vis diffuse reflectance spectra (DRS) (V-670 in Japan) were obtained to determine the band gap energy of the photocatalyst particles.

4. Photocatalytic Activity Test

To assess the photocatalytic activity of the obtained samples, degradation of methylene blue under visible illumination was carried out in a self-designed photocatalytic reactor. The photoreactor was made of a glass tank, with an effective volume of about 1,000 mL. A mechanical stirrer, with the speed of 60 rpm, was used for stirring the dye stock solution. A specified amount of the catalyst (BiOCl-ZnO=0.5 g) was added to 500 mL of the dye diluted solution (Methylene Blue=20 ppm). First, before irradiation, the suspension was stirred for a given time (usually 15-30 min) in the dark to reach adsorption equilibrium, as deduced from steady state concentrations. Then, it was continuously irradiated by a 125 W high pressure mercury lamp (Osrum GmbH, Germany) for 3 h. To filter out most of UV radiation through all radiation spectra of the lamp, a glass bulb with a special cover was used. Thus, the short wave ultraviolet radiations (UV-C and UV-B rays) were mostly retained, and the long wave ultraviolet radiation (UV-A ray) was reduced. The content of the tank was continuously agitated to maintain the experimental environment homogeneous. Specified amounts of the solution were collected, as samples, at equal time intervals, and centrifuged to remove any suspended solid catalyst particles. Finally, these samples were analyzed by UV-vis spectrophotometer (Shimadzu, UV-1601P). The degradation percentage of methylene blue was calculated by using the equation below:

$$\text{Degradation}\ (\%) = \frac{C_o - C}{C_o} \times 100 \quad (1)$$

In which C_o is the initial dye concentration, and C is the dye concentration after treatments.

RESULTS AND DISCUSSION

1. Characterization of BiOCl-ZnO Nanocomposite

The morphologies of pure BiOCl-ZnO and BiOCl-ZnO modified with the surfactants were investigated by SEM, as shown in Fig. 1. The sheet-like and tetragonal characteristic of BiOCl can be clearly seen from this figure [26]. The thickness of prepared BiOCl nanosheets and ZnO nanoparticles was between 50-70 nm and 20-70 nm, respectively (Fig. 1(a) and (b)). As can be seen, the surface of BiOCl sheets is not clean and smooth because of attached ZnO nanoparticles to the sheet surface (Fig. 1(c)). The agglomeration of ZnO particles on the surface of BiOCl, which reduces the uniformity and the photocatalytic active site of the catalyst surface, is obvious in this figure. Consequently, reducing the photocatalytic efficiency, after coupling BiOCl nanosheets with ZnO nanoparticles, is expected. The images of BiOCl-ZnO modified with the surfactants (Fig. 1(d) and (e)) confirm the enhancement of the photocatalyst surface area, as an effective factor for increasing the photocatalytic degradation.

The hydrothermal synthesis, which displays practical applications in the catalytic field, is a strong method for preparing nanocomposites, such as alloys and homogeneous compositions. X-ray diffraction (XRD) pattern of BiOCl-ZnO nanoparticles is demonstrated in Fig. 2. It exhibits typical diffraction peaks corresponding to the hexagonal structure of ZnO and the tetragonal phase of BiOCl, which are in acceptable agreement with the literature values of (JCPDS card no. 80-0075) and (JCPDS card number 06-0249), respectively. The sharp peaks indicate a high degree of crystallization for the products. Furthermore, due to the high content of BiOCl toward ZnO, the peaks of BiOCl are increased. Moreover, no other crystalline impurities were detected, which confirms the high purity of the products.

Fig. 3 shows the FT-IR spectra of BiOCl-ZnO, BiOCl-ZnO-CTAB and BiOCl-ZnO-PEG samples. The peaks at about 525 cm^{-1} and 434 cm^{-1} are attributed to Bi-O stretching mode and Zn-O stretching vibration, respectively [25,27]. The sharp peak at 3,414 cm^{-1} is attributed to O-H bond stretching vibration, which can be related to the adsorbed water on the surface. It is obvious that the diagram

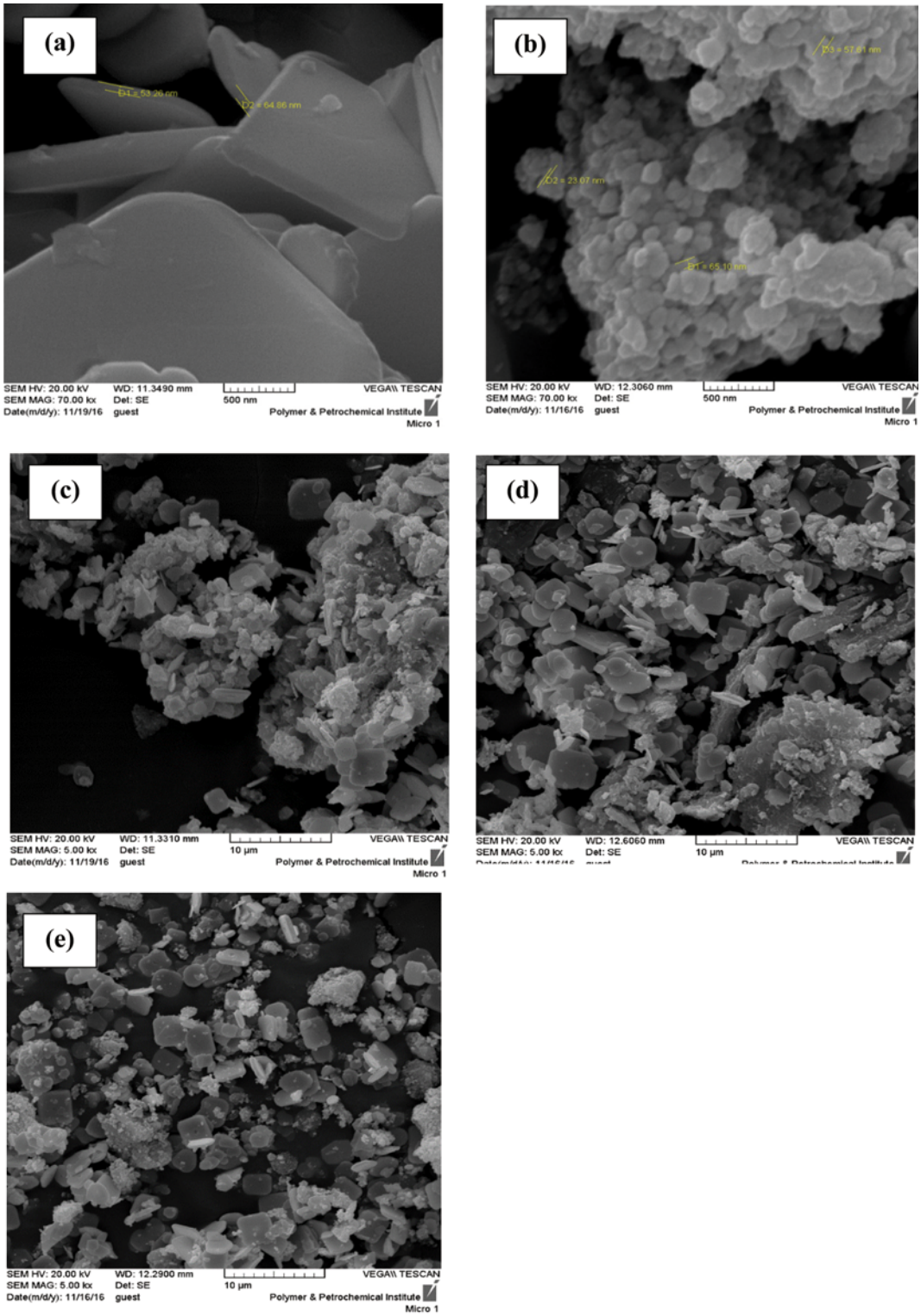

Fig. 1. SEM images of pure BiOCl-ZnO and BiOCl-ZnO modified with the surfactants: (a) BiOCl nanosheets, (b) ZnO nanoparticles, and (c) pure BiOCl-ZnO, (d) BiOCl-ZnO modified with CTAB, and (e) BiOCl-ZnO modified with PEG.

has not changed in desired spectra after removing CTAB by washing the catalyst. Unlike CTAB, PEG is a stable surfactant and cannot be easily washed away from the photocatalyst structure. Moreover, the peaks at 2,365, 1,641 and 1,374 cm^{-1}, corresponding to the stretching vibration of CH_2, carboxylate (COO^-) and -CH, respectively, confirm the presence of PEG in the photocatalyst structure [28].

Fig. 4 presents the UV-vis diffuse reflectance spectra (DRS) of BiOCl-ZnO and BiOCl-ZnO modified with the surfactants. It reveals

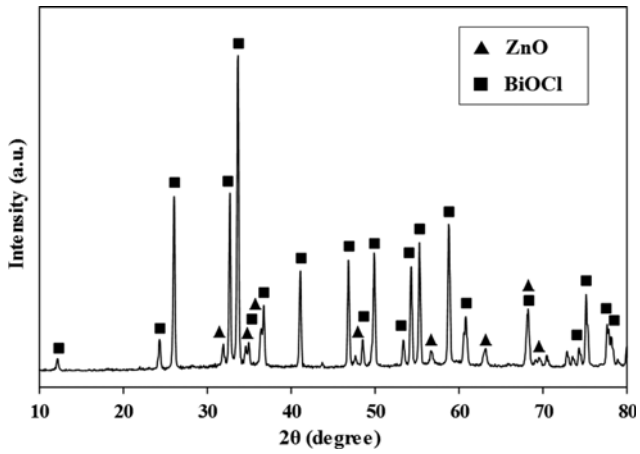

Fig. 2. XRD pattern of BiOCl-ZnO-PEG.

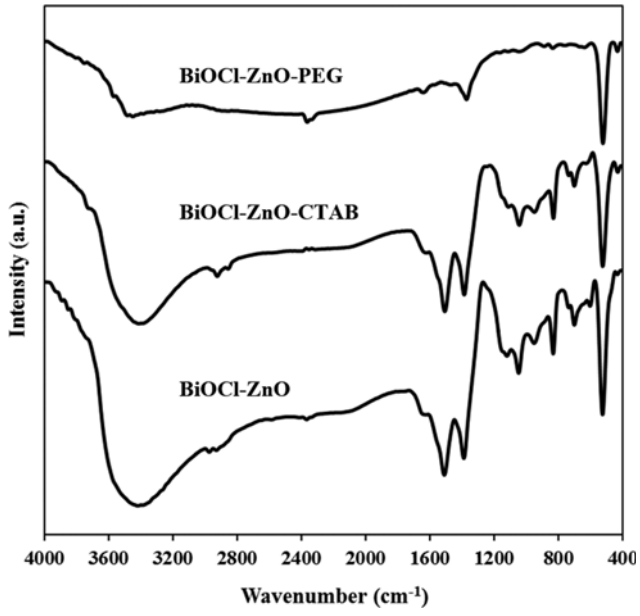

Fig. 3. FTIR spectra of the photocatalysts: pure BiOCl-ZnO, BiOCl-ZnO-CTAB, and BiOCl-ZnO-PEG.

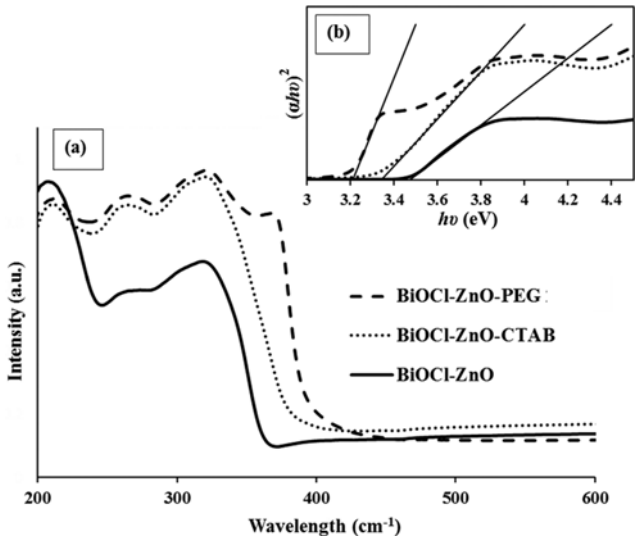

Fig. 4. (a) UV-vis diffuse reflectance spectra of BiOCl-ZnO and BiOCl-ZnO modified with the surfactants. (b) The plot of $(\alpha h\upsilon)^2$ versus photon energy ($h\upsilon$).

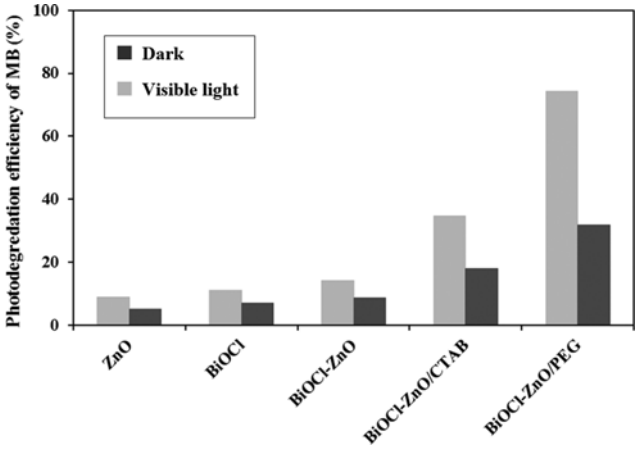

Fig. 5. The degradation efficiency of MB (20 mg/L) catalyzed by different photocatalysts.

that the presence of PEG has more positive effect than CTAB on the absorption peak. This observation has a consistent with the Moradi et al. [29] report. The band gap energy of the samples was computed using Eq. (2).

$$h\upsilon(eV)=\frac{1240}{\lambda} \quad (2)$$

where $h\upsilon$ and λ are the energy (eV) and wavelength (nm) of a photon, respectively. As a result, the calculated band gap energy of BiOCl-ZnO, BiOCl-ZnO-CTAB and BiOCl-ZnO-PEG is 3.55, 3.35 and 3.05 eV, respectively. This observation demonstrates that the incorporation of PEG makes BiOCl-ZnO as a visible light responsive photocatalyst.

2. Photocatalytic Performance

To assess the effect of the surfactants on photocatalytic properties of the prepared photocatalysts, the photocatalytic degradation of methylene blue was carried out under visible light illumination. The activity of synthesized BiOCl-ZnO modified with the surfactants (PEG and CTAB), compared with the pure BiOCl, ZnO, and BiOCl-ZnO samples, is illustrated in Fig. 5. It is obvious that the photocatalytic performance of BiOCl-ZnO-PEG is better than that of BiOCl-ZnO-CTAB, BiOCl-ZnO nanoparticles, and pure BiOCl and ZnO, in the both presence and absence of irradiation.

3. Kinetic of MB Disappearance

The kinetic of MB disappearance by three synthesized catalysts is discussed in Fig. 6. It follows an apparent first-order kinetic model, which is in agreement with the linear transformation of $-\ln(C/C_o)=f(t)$. In this regard, the Langmuir-Hinshelwood mechanism was used as follows (Eq. (3)):

$$r=k\theta=\frac{kKC}{1+KC}\approx kKC=k_{app}C \quad (3)$$

where r is the rate of a reaction (mg/L min), K is the rate constant

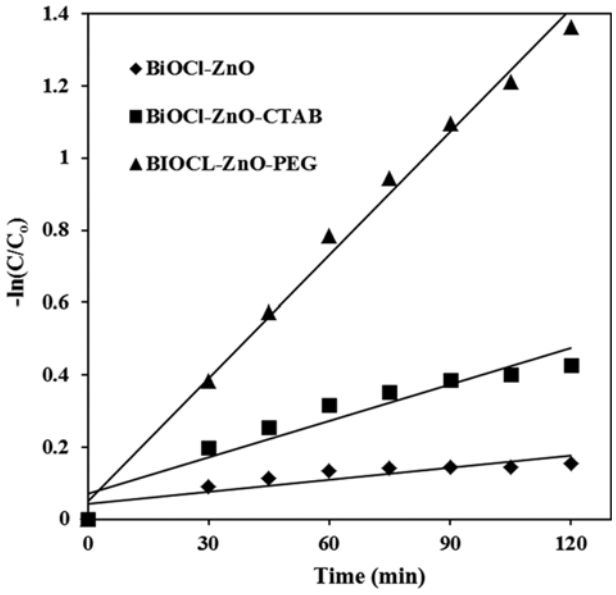

Fig. 6. The Langmuir-Hinshelwood kinetic in the photocatalytic degradation of MB by three synthesized catalysts (BiOCl-ZnO, BiOCl-ZnO-CTAB and BiOCl-ZnO-PEG).

Table 1. The kinetic parameters of MB photodegradation

Photocatalyst	Photodegradation efficiency of MB (%)	K	R^2
BiOCl-ZnO-PEG	74.4	0.011	0.992
BiOCl-ZnO-CTAB	34.72	0.003	0.909
BiOCl-ZnO	14.24	0.001	0.777

of photocatalysis (mg/L min), k is the rate constant of the reaction (L/mg), and C is the concentration of methylene blue (mg/L) at any time of t (min). Table 1 shows the removal efficiencies, rate constants and R^2 of BiOCl-ZnO-CTAB, BiOCl-ZnO-PEG and BiOCl-ZnO after 120 min of visible light irradiation. It was observed that the rate constant of BiOCl-ZnO-PEG was higher than that of both BiOCl-ZnO-CTAB and BiOCl-ZnO. This is due to more photocatalytic activity of BiOCl-ZnO-PEG toward BiOCl-ZnO-CTAB and BiOCl-ZnO under visible light irradiation as discussed earlier.

4. Effect of Initial Concentration of MB

The effect of varying the initial dye concentration from 10 to 30 ppm on the photocatalytic degradation of methylene blue is exhibited in Fig. 7. The experiments were done in natural pH and catalyst dosage of 1 g/L. As can be seen, the rate of photocatalytic degradation increases with increasing the concentration of the dye from 10 to 20 ppm. It is owing to the probability enhancement of the interaction between extra methylene blue molecules near the surface and the oxidizing species, which leads to an increase in the degradation efficiency. In contrast, by increasing the initial dye concentration up to 30 mg/L, the degradation efficiency clearly decreases. Owing to the absorbance of light photons by pollutant molecules in the solution, the production of the charge carriers is faced with serious restrictions through the lack of sufficient light for activation of the catalyst. On the other hand, this further increase in the initial dye concentration causes more adsorption of methylene blue molecules on the photocatalyst surface, which not only results in occupancy of more active sites, but also is a barrier for direct accessing of hydroxide ions and oxygen molecules to the catalyst surface. Hence, the generation of $OH^{\bullet}$ and $O_2^{-\bullet}$ radicals, which are required for the degradation of methylene blue molecules, decreases. Consequently, the higher the initial concentration of methylene blue (more than 20 ppm) the lower the degradation efficiency.

5. Effect of Catalyst Dosage

The effect of the photocatalyst dosage on the photodegradation of the dye was studied in the range of 0.5-1.5 g/L. The experiment was done at the natural pH, and the initial dye concentration of 20 ppm. The results are shown in Fig. 8. As can be concluded, by altering the photocatalyst dosage from 0.5 to 1 g/L, the degradation efficiency increases and reaches its maximum value at 1 g/L. increasing the necessary catalytic active surface by increasing the catalyst dosage can explain this observation. However, by adding the catalyst dosage more than 1 g/L, the degradation efficiency decreases. It is due to the overlapping of catalyst particles, and the opac-

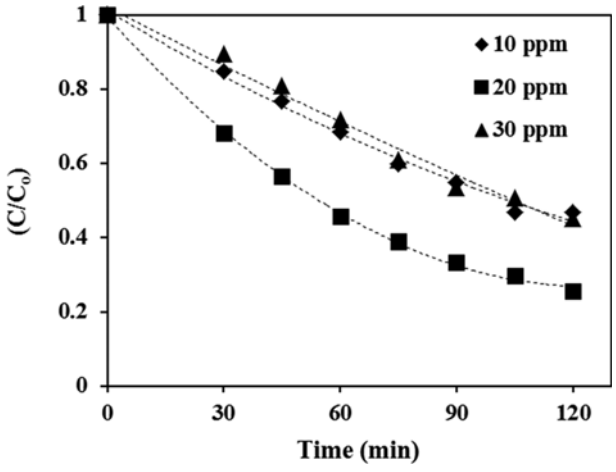

Fig. 7. The effect of MB initial concentration on the degradation efficiency of MB at natural pH and BiOCl-ZnO-PEG dosage of 1 g/L.

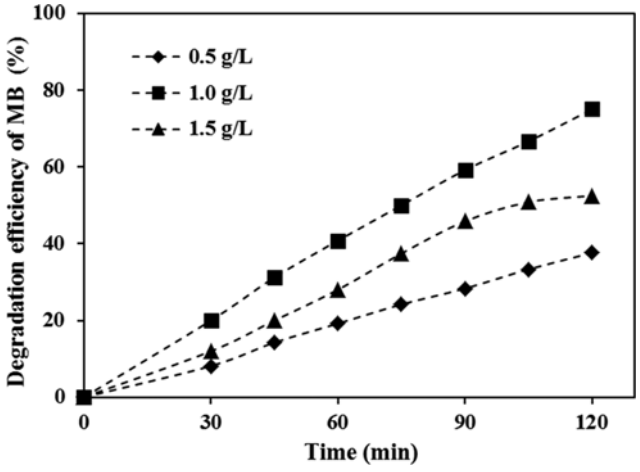

Fig. 8. The effect of BiOCl-ZnO-PEG dosage on the degradation efficiency of MB at natural pH and MB initial concentration of 20 ppm.

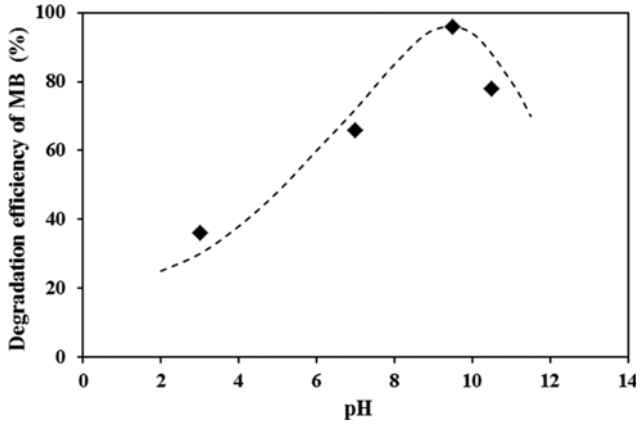

Fig. 9. The effect of pH value on the degradation efficiency of MB at BiOCl-ZnO-PEG dosage of 1 g/L and MB initial concentration of 20 ppm.

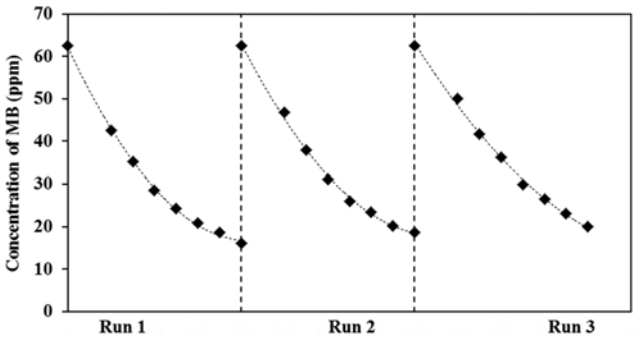

Fig. 10. The degradation efficiency of MB by BiOCl-ZnO-PEG photocatalyst after three repetitions.

ity of the reaction environment, which prevents from reaching sufficient light to the catalyst surface, and producing the oxidizing species. Hence, the optimum value of 1 g/L BiOCl-ZnO-PEG was used in the next investigations.

6. Effect of pH

pH of a solution is a key parameter in a photocatalytic reaction. The pH values influence the electrostatic interaction between a catalyst surface and contaminant molecules (MB), the concentration of generated hydroxyl radicals and the reaction of superoxide and hydroxyl radicals, which are formed on the catalyst surface, with contaminant species. The surface coverage and the absorption behavior of a nanoparticle depend on its iso-electronic point. When pH is lower than its isoelectric point (IEP), the surface charge of the nanoparticle will be positive. In contrast, at higher pH values, it is negatively charged [30]. Therefore, the degradation strongly depends on pH of the solution. In this study, the influence of pH alteration in the range of 3 to 10 on the degradation of MB dye was investigated, and the results are shown in Fig. 9. In this part, the catalyst dosage, and the initial concentration of dye were considered 1 g/L and 20 ppm, respectively. In all experiments, pH was adjusted by adding an appropriate amount of 0.01 N HCl or 0.01 N NaOH solutions. It is obvious that the adsorption capacity increases by increasing pH values up to 9.5. MB is a cationic dye, and exists in the form of positively charged ions in an aqueous medium. Thus, in an acidic solution, a competition takes place between excess H_3O^+ ions and dye cations, which causes a decrease in the adsorption capacity, and minimizes the degradation rate. At high values of pH, although the negative surface charge will hinder the creation of holes, the formation of $OH^•$, via oxidation of OH^-, becomes convenient. Therefore, positively charged MB ions can locate at adsorbent sites, and generate a highly concentrated environment around the catalyst, which causes relatively high degradation efficiency. At pH values higher than 9.5, the dye degradation is inhibited because of the competition between hydroxyl ions and dye molecules in the adsorption process on the catalyst surface. As a result, the degradation efficiency is reduced [31].

7. Stability of the Photocatalyst

Stability of photocatalysts is a very important factor for industrial applications. In this study, it was examined by reusing the consumed BiOCl-ZnO-PEG nanocomposite in the degradation experiments of MB under same conditions for three times. For this purpose, after centrifugal separation, the catalyst was washed with distilled water and immediately reused for more runs without any treatment. The results are shown in Fig. 10. In accordance with this figure, only a slight decrease, by about 8.5%, is found after three repetitions, which is most likely because of washing some of PEG molecules from the structure of the photocatalyst. These observations prove the excellent reusable performance and considerable stability of the catalyst, which maintains the photocatalytic efficiency high.

CONCLUSIONS

We investigated the effect of different surfactants, such as CTAB and PEG, on the performance of BiOCl-ZnO nanoparticle, as a photocatalyst for the organic pollutant removal under visible light. It is concluded that the performance of PEG in the structure of BiOCl-ZnO nanoparticles is more effective than CTAB. This may be because of the coverage of nanoparticles by PEG molecules, as a polymer layer. They create middle levels between conduction and valence bands of the nanoparticles, which reduces the bandgap energy, and causes the activation of the photocatalysts in the visible region. In the survey of the effect of methylene blue concentration, catalyst dosage and solution pH, the optimum conditions were 20 ppm, 1 g/L and 9.5, respectively. Photodegradation of methylene blue using BiOCl-ZnO-PEG photocatalyst at optimal conditions indicated that 96.3% of methylene blue can be removed in a short period of irradiation time. Moreover, this catalyst demonstrated considerable stability, and maintained its photocatalytic efficiency high after three replications.

REFERENCES

1. C. T. Helmes, C. C. Sigman, V. A. Fung, K. Thompson, M. K. Doeltz, M. Mackie, T. E. Klein and D. Lent, *J. Environ. Sci. Health, Part A: Toxic/Hazard. Subst. Environ. Eng.*, **19**, 97 (1984).
2. P. Simon, *Advanced oxidation processes for water and wastewater treatment*, March, IWA Publishing (2004).
3. M. M. Alnuaimi, M. A. Rauf and S. S. Ashraf, *Dyes Pigm.*, **72**, 367

(2007).
4. Y. Shaveisi and S. Sharifnia, *J. Energy Chem.*, **27**, 290 (2018).
5. G. Moussavi and M. Mahmoudi, *Chem. Eng. J.*, **152**, 1 (2009).
6. M. A. Rauf, M. A. Meetani, A. Khaleel and A. Ahmed, *Chem. Eng. J.*, **157**(2-3), 373 (2010).
7. J. H. Sun, S. P. Sun, G. L. Wang and L. P. Qiao, *Dyes Pigm.*, **74**, 647 (2007).
8. T. Yonar, *Decolorisation of textile dyeing effluents using advanced oxidation processes*, INTECH Open Access Publisher (2011).
9. Y. Shavisi, S. Sharifnia, S. N. Hosseini and M. A. Khadivia, *J. Ind. Eng. Chem.*, **20**(5), 2806 (2014).
10. J. Yang, X. Wang, X. Lv, X. Xu, Y. Mi and J. Zhao, *Ceram. Int.*, **40**(6), 8607 (2014).
11. X. F. Chang, M. A. Gondal, A. A. Al-Saadi, M. A. Ali, H. F. Shen, Q. Zhou, J. Zhang, M. P. Du, Y. S. Liu and G. B. Ji, *J. Colloid Interface Sci.*, **377**, 291 (2012).
12. M. A. Gondal, X. F. Chang, M. A. Ali, Z. H. Yamani, Q. Zhou and G. B. Ji, *Appl. Catal. A*, **397**, 192 (2011).
13. Z. S. Liu, B. T. Wu, D. H. Xiang and Y. B. Zhu, *Mater. Res. Bull.*, **47**, 3753 (2012).
14. B. Pare, B. Sarwan and S. B. Jonnalagadda, *Appl. Surf. Sci.*, **258**, 247 (2011).
15. B. Sarwan, B. Pare, A. D. Acharya and S. B. Jonnalagadda, *J. Photochem. Photobiol. B*, **116**, 48 (2012).
16. S. Shenawi-Khalil, V. Uvarov, Y. Kritsman, E. Menes, I. Popov and Y. Sasson, *Catal. Commun.*, **12**, 1136 (2011).
17. J. X. Xia, S. Yin, H. M. Li, H. Xu, L. Xu and Q. Zhang, *Colloids Surf. A*, **387**, 23 (2011).
18. L. Zhao, X. Zhang, C. Fan, Z. Liang and P. Han, *Phys. B*, **407**(17), 3364 (2012).
19. Z. Q. Shi, Y. Wang, C. Fan, Y.-f. Wang and G. Ding, *Trans. Nonferrous Metals Soc. Chin.*, **21**(10), 2254 (2011).
20. K. L. Zhang, C. M. Liu, F. Q. Huang, C. Zheng and W. D. Wang, *Appl. Catal. B*, **68**, 125 (2006).
21. P. S. J. Henle, A. Frenzel, S. Scholz and S. Kaskel, *Chem. Mater.*, **19**(3), 366 (2007).
22. X. Zhang, F. L. Jia and L. Z. Zhang, *J. Phys. Chem. C*, **112**(3), 747 (2008).
23. Y. Yu, *J. Mater. Chem. A*, **2**, 1677 (2014).
24. Y. Li, C. Li, X. Sun, Z. Zhang, Z. Peng, J. Zhang and J. Zhao, *Mater. Lett.*, **116**, 98 (2014).
25. M. Yousefi, E. Noori, D. Ghanbari, M. Salavati-Niasari and T. Gholami, *J. Cluster Sci.*, **25**, 397 (2014).
26. J. Jiang, K. Zhao, X. Xiao and L. Zhang, *J. Am. Chem. Soc.*, **134**(10), 4473 (2012).
27. T. X. Tao, G. S. Dai, J. B. Xu, W. Chu and Z. C. Wu, *Mater. Res. Innovations*, **20**, 216 (2016).
28. S. Amala Jayanthi, D. Sukanya, A. Joseph Arul Pragasam and P. Sagayaraj, *Der Pharma Chemica*, **5**, 90 (2013).
29. S. Moradi, M. Vossoughi, M. Feilizadeh, S. M. E. Zakeri, M. M. Mohammadi, D. Rashtchian and A. Yoosefi Booshehri, *Res. Chem. Intermed.*, **41**, 4151 (2015).
30. D. Zhang and F. Zeng, *J. Mater. Sci.*, **47**, 2155 (2012).
31. H. R. Pouretedal and A. Kadkhodaie, *Chin. J. Catal.*, **31**, 1328 (2010).